

## Effect of Relative Humidity on Arctic Aerosols

\*G.S.M. Galadanci<sup>1</sup> and B. I. Tijjani<sup>2</sup>

1. (Presently) Department of Physics, Federal University, Dutse, Jigawa State Nigeria
2. Department of Physics, Bayero University, Kano P.M.B 3011, Kano. Nigeria

\* E-mail of the corresponding author: [gsmgalad@gmail.com](mailto:gsmgalad@gmail.com),

### Abstract

In this paper, the authors investigated some microphysical and optical properties of arctic aerosols extracted from the data base Optical Properties of Aerosols and Clouds(OPAC) to determine the effect of hygroscopic growth at the spectral range of 0.25 $\mu$ m to 2.5 $\mu$ m and eight relative humidities (RHs) (0, 50, 70, 80, 90, 95, 98, and 99%). The microphysical properties extracted were radii, volume mix ratio, number mix ratio and mass mix ratio as a function of RH while the optical properties are scattering and absorption coefficients and asymmetric parameters. Using the microphysical properties, effective growth factors of the mixtures were determined while using optical properties enhancement parameters were determined and then parameterized using some models. We observed that the data fitted the models very well. The angstrom coefficients which determined the type of particles size distribution increases with the increase in RHs except at the delinquent point where it decreases with the increase in RHs. The mixture was determined to have bimodal type of distribution with the dominance of fine mode particles but non-spherical.

**Keywords:** microphysical properties, optical properties, hygroscopic growth, enhancement parameters, models, parametrisation.

### 1 Introduction

The Arctic is a polar region located at the northernmost part of the Earth which is a unique area among Earth's ecosystems. The Arctic region consists of a vast, ice-covered ocean, surrounded by treeless permafrost.

The aerosol hygroscopic properties are very crucial for the understanding of the aerosol effects on climate via their effects on clouds. The hygroscopic growth measured at sub saturation is closely related to the ability of aerosol particles to activate and form cloud droplets (Swietlicki et al., 2008; Rissler et al., 2010).

Generally, hygroscopic solutes grow significantly in size at high RH due to water uptake, and hence influence the aerosol optical and microphysical properties as well as their physical and chemical characteristics (Cheng et al., 2008; Topping et al., 2005a, b). Recently, several single-parameter schemes have been proposed to simplify the Kohler equation (Kohler, 1936). Hygroscopicity parameter,  $\kappa$  and ions density,  $\rho_{ion}$  have been defined as proxies of chemical composition to represent aerosol hygroscopic growth as well as the ability of aerosol particles to become cloud condensation nuclei (CCN) (Petters and Kreidenweis, 2007; Wex et al., 2007).

Virtually every property of atmospheric aerosols is a strong function of Relative Humidity (RH). Changes in particle size and phase with relative humidity modify heterogeneous atmospheric chemistry, cloud and fog formation processes, and visibility. As climate models improve, they must incorporate the dependence of aerosol radiative effects on RH. Because of the important role that water vapor plays in determining aerosol effects it is critical to develop the understanding that is required to reliably represent water vapor-particle interactions in models. With increasing RH particles containing hygroscopic salts and acids grow and become solution droplets, whereas particles composed of soot, or dust particles materials may not grow significantly with increasing RH.

The main parameter used to characterize the hygroscopicity of the aerosol particles is the aerosol hygroscopic growth factor  $gf(RH)$ , which is defined as the ratio of the particle diameter at any RH to the particle diameter at  $RH = 0\%$  (Kammermann et al., 2010; Swietlicki et al., 2008).

Changes in the aerosol optical properties resulting from the particle hygroscopic growth are described by enhancement factors  $f(\lambda, RH)$ , which, for each optical parameter  $\chi(\lambda, RH)$ , are defined as the ratio between its values determined in any conditions  $\chi(\lambda, RH)$  and those determined in dry conditions  $\chi(\lambda, RH = 0\%)$ .

The aim of this study is to determine the effect of RH and wavelength on the globally averaged direct aerosol for arctic aerosols from the data extracted from OPAC. One or two variables parameterizations models will be performed to determine the relationship of the particles' hygroscopic growth and enhancement parameters with the RH. Angstrom coefficients are used to determine the particles' type and the changes in the mode size and type distribution as a result of the changes in RHs.

## 2 METHODOLOGY

The models extracted from OPAC are given in table 1.

Table 1: The microphysical properties of the aerosols at 0% RH (Hess et al., 1998).

| Components | No.Conc.(cm <sup>-3</sup> ) | R <sub>min</sub> (μm): | R <sub>max</sub> (μm): | sigma: | R <sub>mod</sub> (μm): |
|------------|-----------------------------|------------------------|------------------------|--------|------------------------|
| Inso       | 0.0100                      | 0.0050                 | 20.0000                | 2.5100 | 0.4710                 |
| Waso       | 1,300.0000                  | 0.0050                 | 20.0000                | 2.2400 | 0.0212                 |
| Soot       | 5,300.0000                  | 0.0050                 | 20.0000                | 2.0000 | 0.0118                 |
| Ssam       | 1.9000                      | 0.0050                 | 20.0000                | 2.0300 | 0.2090                 |

The aerosol's hygroscopic growth factor  $gf(RH)$ , (Swietlicki et al., 2008; Randles, et al., 2004) is defined as:

$$gf(RH) = \frac{D(RH)}{D(RH=0)} \quad (1)$$

where RH is taken for seven values 50%, 70%, 80%, 90%, 95%, 98% and 99%.

But since atmospheric aerosols consist of more and less hygroscopic sub fractions so the information on the hygroscopicity modes was merged into an "over-all" or "bulk" hygroscopic growth factor of the mixture,  $gf_{mix}(RH)$ , representative for the entire particle population as:

$$gf_{mix}(RH) = (\sum_k x_k gf_k^3)^{1/3} \quad (2)$$

The effective or volume equivalent radius of the mixture was determined using the relation

$$r_{effec}(RH) = (\sum_k x_k r_k^3)^{1/3} \quad (3)$$

where the summation is performed over all compounds present in the particles and  $x_k$  represent their respective volume fractions, using the Zdanovskii-Stokes-Robinson relation (ZSR relation; Sjogren et al., 2007; Stokes and Robinson, 1966; Meyer et al., 2009; Stock et al., 2011). Solute-solute interactions are neglected in this model and

volume additivity is also assumed. The model assumes spherical particles, ideal mixing (i.e. no volume change upon mixing) and independent water uptake of the organic and inorganic components.

Equation (5) was also be computed using the  $x_k$  as the corresponding number fractions (Duplissy et al., 2011; Meier et al., 2009).

We now proposed the  $x_k$  to represent the mass mix ratio of the individual particles. The RH dependence of  $gf_{mix}(RH)$  can be parameterized in a good approximation by a one-parameter equation, proposed e.g. by Petters and Kreidenweis(2007) as:

$$gf_{mix}(a_w) = \left(1 + \kappa \frac{a_w}{1-a_w}\right)^{\frac{1}{3}} \quad (4)$$

Here,  $a_w$  is the water activity, which can be replaced by the relative humidity RH, if the Kelvin effect is negligible, as for particles with sizes more relevant for light scattering and absorption. The coefficient  $\kappa$  is a simple measure of the particle's hygroscopicity and captures all solute properties (Raoult effect), that is, it is for the ensemble of the particle which can be defined in terms of the sum of its components. In an ensemble of aerosol particles, the hygroscopicity of each particle can be described by an "effective" hygroscopicity parameter  $\kappa$  (Petters and Kreidenweis, 2007). Here "effective" means that the parameter accounts not only for the reduction of water activity by the solute but also for surface tension effects (Rose et al., 2008; Gunthe et al., 2009; Poschl et al., 2009). It also scales the volume of water associated with a unit volume of dry particle (Petters and Kreidenweis, 2007) and depends on the molar volume and the activity coefficients of the dissolved compounds (Christensen and Petters, 2012). The  $\kappa$  value derived for a particle of a given composition may vary, depending upon the size molar mass, the activity and RH it is derived at.

For atmospheric aerosols, the range of  $\kappa$  typically varies from as low as  $\sim 0.01$  for some combustion aerosol particles up to  $\sim 1$  for sea-salt particles (Petters and Kreidenweis, 2007; Petters et al., 2009a).

The following sub-divisions at 85% RH were made by Liu et al., 2011 and Swietlicki et al., (2008); as: nearly-hydrophobic particles (NH):  $\kappa \leq 0.10$  ( $gf_{mix} \leq 1.21$ ), less-hygroscopic particles (LH):  $\kappa = 0.10 - 0.20$  ( $gf_{mix} = 1.21 - 1.37$ ); more-hygroscopic particles (MH):  $\kappa > 0.20$  ( $gf_{mix} > 1.37$ ).

Making  $\kappa$  as the subject of the equation (4), we get

$$k(a_w) = \frac{[gf_{mix}^3(a_w) - 1](1 - a_w)}{a_w} \quad (5)$$

Humidograms of the ambient aerosols obtained in various atmospheric conditions showed that  $gf_{mix}(RH)$  could as well be fitted well with a  $\gamma$ -law (Swietlicki et al., 2008; Birmili et al., 2004; Kasten, 1969; Gysel et al., 2009; Putaud, 2012) as

$$gf_{mix}(RH) = (1 - RH)^\gamma \quad (6)$$

Making  $\gamma$  as the subject of equation (6) we get

$$\gamma(RH) = \frac{\ln(gf_{mix}(RH))}{\ln(1 - RH)} \quad (7)$$

The bulk hygroscopicity factor B under subsaturation RH conditions was determined using the relation:

$$B = (1 - gf_{mix}^3) \ln a_w \quad (8)$$

where  $a_w$  is the water activity, which can be replaced by the RH as explained before.

The impact of hygroscopic growth on the optical properties of aerosols is usually described by the enhancement

factor  $f_x(RH, \lambda)$ :

$$f_x(RH, \lambda) = \frac{\chi(RH, \lambda)}{\chi(RH_{ref}, \lambda)} \quad (9)$$

where in our study  $RH_{ref}$  was 0%, and RH was taken for seven values of 50%, 70%, 80%, 90%, 95%, 98% and 99%.

In general the relationship between  $f_x(RH, \lambda)$  and RH is nonlinear (e.g. Jeong et al. 2007). In this paper we

determine the empirical relations between the enhancement parameter and RH (Doherty et. al., 2005) as:

$$f_x(RH, \lambda) = \frac{\chi(RH, \lambda)}{\chi(RH_{ref}, \lambda)} = \left( \frac{100 - RH_{ref}}{100 - RH} \right)^\gamma \quad (10)$$

The  $\gamma$  known as the humidification factor represents the dependence of aerosol optical properties on RH, which results from the changes in the particles sizes and refractive indices upon humidification. The use of  $\gamma$  has the advantage of describing the hygroscopic behavior of aerosols in a linear manner over a broad range of RH values; it also implies that particles are deliquesced (Quinn et al., 2005), a reasonable assumption for this data set due to the high ambient relative humidity during the field study. The  $\gamma$  parameter is dimensionless, and it increases with increasing particle water uptake.

Making  $\gamma$  as the subject of equation(10) and  $RH_{ref} = 0$ , we get

$$\gamma(RH, \lambda) = - \frac{\ln(f_x(RH, \lambda))}{\ln(1 - RH)} \quad (11)$$

From previous studies, typical values of  $\gamma$  for ambient aerosol ranged between 0.1 and 1.5 (Gasso et. al., 2000; Quinn et al., 2005; Clarke et al., 2007). Two parameters empirical relation was also used (Jeong et. al., 2007; Hanel, (1976)) as;

$$f_x(RH, \lambda) = a(1 - RH)^b \quad (12)$$

Equations (12) and (14) are verified at wavelengths 0.25, 0.45, 0.55, 0.70, 1.25, and 2.50  $\mu\text{m}$ .

To determine the effect of particles distributions as a result of change in RH and soots, the Angstrom exponent was determined using the spectral behavior of the aerosol optical depth, with the wavelength of light ( $\lambda$ ) was expressed as inverse power law (Angstrom, 1961):

$$\tau(\lambda) = \beta \lambda^{-\alpha} \quad (13)$$

The Angstrom exponent was obtained as a coefficient of the following regression,

$$\ln \tau(\lambda) = -\alpha \ln(\lambda) + \ln \beta \quad (14)$$

However equation (14) was determined as non-linear ( that is the Angstrom exponent itself varies with wavelength), and a more precise empirical relationship between the optical depth and wavelength was obtained with a second-order polynomial (King and Byrne, 1976; Eck et al., 1999; Eck. et al., 2001a, b.; Kaufman, 1993; O'Neill et al., 2001a, 2003; Pedros et al, 2003; Kaskaoutis and Kambezidis, 2006; Schmid et al., 2003; Martinez-Lozano et al., 2001) as:

$$\ln \tau(\lambda) = \alpha_2 (\ln \lambda)^2 + \alpha_1 \ln \lambda + \ln \beta \quad (15)$$

then we proposed the cubic relation to determine the type of mode distribution as:

$$\ln X(\lambda) = \ln \beta + \alpha_1 \ln \lambda + \alpha_2 (\ln \lambda)^2 + \alpha_3 (\ln \lambda)^3 \quad (16)$$

where  $\beta$ ,  $\alpha$ ,  $\alpha_1$ ,  $\alpha_2$ ,  $\alpha_3$  are constants that were determined using regression analysis with SPSS16.0. for windows.

We also determined the exponential dependence of the aerosol optical thickness on relative humidity as done by Jeong et al. (2007) as;

$$\tau(RH) = A e^{B(RH/100)} \quad (17)$$

where A and B are constants determined using regression analysis with SPSS 16.0. Equation (17) was computed at wavelengths 0.25, 1.25 and 2.50  $\mu\text{m}$ .

We finally determine the effect of hygroscopic growth and change in the change in the concentration of soot on the effective refractive indices of the mixed aerosols using the following formula (Aspens, 1982):

$$\frac{\varepsilon_{eff} - \varepsilon_0}{\varepsilon_{eff} + 2\varepsilon_0} = \sum_{i=1}^n f_i \frac{\varepsilon_i - \varepsilon_0}{\varepsilon_i + 2\varepsilon_0} \quad (18)$$

where  $f_i$  and  $\varepsilon_i$  are the volume fraction and dielectric constant of the  $i^{\text{th}}$  component and  $\varepsilon_0$  is the dielectric constant of the host material.

The relation between dielectrics and refractive indices is

$$m_i = \sqrt{\varepsilon_i} \quad (19)$$

For the case of Lorentz-Lorentz (Lorentz, 1880; Lorentz, 1880), the host material is taken to be vacuum,  $\varepsilon_0 = 1$ .

We then proposed the  $f_i$  to be mass mix ratio and number mix ratio, to determine the advantage of one over the other.

The volume-mixing rule calculates the effective refractive index ( $m$ ) of a mixture as the sum of the refractive index ( $m_j$ ) of each component  $j$  weighted by its corresponding volume fraction ( $V_j$ ), (Heller, 1945) as ,

$$m = \sum_{j=1}^n V_j m_j \quad (20)$$

This mixing rule is used in the several widely employed databases of aerosol optical properties (Wang and Martin (2007); Shettle and Fenn, 1979; d'Almeida et al., 1991; Hess et al., 1998).

The computation of equations (18), (19) and (20) were done using the complex functions of Microsoft Excel 2010.

### 3 Results and Discussions

Table 2: the table of growth factors of the mixtures effective radii, bulk hygroscopicity, hygroscopicity and  $\gamma$ , of the aerosols using number mix ratio.

| RH(%)          | 0      | 50      | 70      | 80      | 90      | 95      | 98      | 99      |
|----------------|--------|---------|---------|---------|---------|---------|---------|---------|
| $gf_{mix}(RH)$ | 1.0000 | 1.0554  | 1.0866  | 1.1179  | 1.1882  | 1.2851  | 1.4499  | 1.5848  |
| $R_{eff}$      | 0.0182 | 0.0252  | 0.0278  | 0.0303  | 0.0356  | 0.0427  | 0.0555  | 0.0680  |
| B              |        | 0.1218  | 0.1009  | 0.0886  | 0.0714  | 0.0576  | 0.0414  | 0.0300  |
| $\kappa$       |        | 0.1757  | 0.1212  | 0.0993  | 0.0753  | 0.0591  | 0.0418  | 0.0301  |
| $\gamma$       |        | -0.0778 | -0.0690 | -0.0693 | -0.0749 | -0.0837 | -0.0950 | -0.1000 |

From Table 2, it can be observe that  $gf_{mix}(RH)$  and  $R_{eff}$  increase with the increase in RH, B and  $\kappa$  decrease with the increase in RH while  $\gamma$  fluctuates with the increase in RH.

The results of the parameterizations by one parameter of equations (4) and (6) using number mix ratios are:

$$\kappa=0.0336, R2= 0.9478 \quad (\text{from equation (4)})$$

$$\gamma= -0.0911, R2= 0.9875 \quad (\text{from equation( 6)})$$

From the observations  $R^2$ , it can be seen that the data fitted the equations very well.

Table 3: The ttable of growth factors of the mixtures effective radii, bulk hygroscopicity, hygroscopicity and  $\gamma$ , of the aerosols using volume mix ratio.

| RH(%)          | 0      | 50      | 70      | 80      | 90      | 95      | 98      | 99      |
|----------------|--------|---------|---------|---------|---------|---------|---------|---------|
| $gf_{mix}(RH)$ | 1.0000 | 1.4542  | 1.6385  | 1.8074  | 2.1699  | 2.6565  | 3.5491  | 4.4463  |
| $R_{eff}$      | 0.2075 | 0.2867  | 0.3232  | 0.3574  | 0.4331  | 0.5360  | 0.7262  | 0.9173  |
| B              |        | 1.4384  | 1.2122  | 1.0943  | 0.9711  | 0.9103  | 0.8830  | 0.8734  |
| $\kappa$       |        | 2.0752  | 1.4566  | 1.2260  | 1.0241  | 0.9340  | 0.8920  | 0.8778  |
| $\gamma$       |        | -0.5402 | -0.4101 | -0.3678 | -0.3364 | -0.3261 | -0.3238 | -0.3240 |

From Table 3, it can be observe that  $gf_{mix}(RH)$  and  $R_{eff}$  increase with the increase in RH, B and  $\kappa$  decrease with the increase in RH while  $\gamma$  fluctuates with the increase in RH.

The results of the parameterizations by one parameter of equations (4) and (6) using volume mix ratio are:

$$k=0.8838, R2= 0.9992 \quad (\text{from equation (4)})$$

$$\gamma=-0.3316, R2=0.9940 \quad (\text{from equation (6)})$$

From the observations of  $R^2$ , it can be seen that the data fitted the equations very well.

Table 4: the Table of growth factors, of the mixtures effective radii, bulk hygroscopicity, hygroscopicity and  $\gamma$ , of the aerosols using mass mix ratio.

| RH(%)     | 0      | 50      | 70      | 80      | 90      | 95      | 98      | 99      |
|-----------|--------|---------|---------|---------|---------|---------|---------|---------|
| gfmix(RH) | 1.0000 | 1.4480  | 1.6281  | 1.7947  | 2.1560  | 2.6423  | 3.5359  | 4.4340  |
| $R_{eff}$ | 0.2164 | 0.2887  | 0.3226  | 0.3554  | 0.4300  | 0.5325  | 0.7229  | 0.9144  |
| B         |        | 1.4115  | 1.1826  | 1.0668  | 0.9506  | 0.8950  | 0.8729  | 0.8661  |
| $\kappa$  |        | 2.0363  | 1.4210  | 1.1952  | 1.0025  | 0.9183  | 0.8818  | 0.8704  |
| $\gamma$  |        | -0.5341 | -0.4048 | -0.3634 | -0.3337 | -0.3243 | -0.3228 | -0.3234 |

From Table 4, it can be observe that  $g_{mix}(RH)$  and  $R_{eff}$  increase with the increase in RH, B and  $\kappa$  decrease with the increase in RH while  $\gamma$  fluctuates with the increase in RH.

The results of the parameterizations by one parameter of equations (4) and (6) are:

$$k = 0.8755, R^2 = 0.9993 \quad (\text{from equation (4)})$$

$$\gamma = -0.3302, R^2 = 0.9945 \quad (\text{from equation (6)})$$

From the observations of  $R^2$ , it can be seen that the data fitted the equations very well.

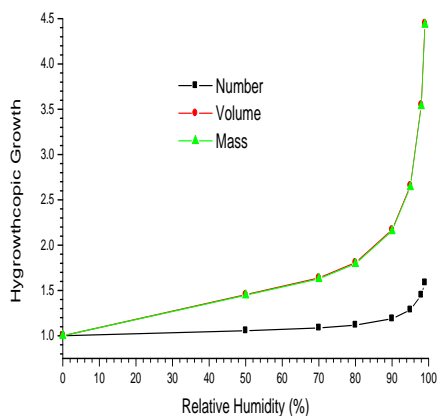


Figure 1. A graph of Hygroscopic Growth against Relative Humidity From the Data of Tables 2, 3 and 4.

From figure 1, it can be observe that all the plots can satisfy power law, and the plots using volume and mass mix ratios have higher values compared to using number mix ratios. Though volume mix-ratio is the highest with only a slight increase of between 0.01 to 0.02 compared with mass mix-ratio.

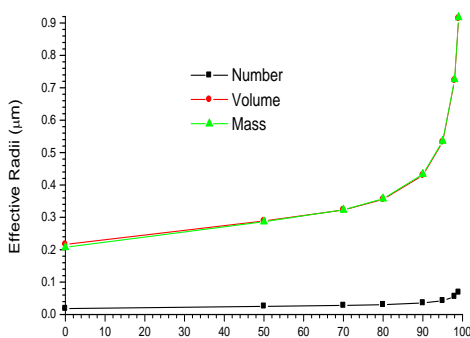


Figure 2. A graph of Effective Radii against Relative Humidity From the Data of Tables 2, 3 and 4.

From Figure 2, it can be observe that all the plots can satisfy power law, and the plots using volume and mass

mix ratios have higher values compared to using number mix ratios. Though volume mix-ratio is the highest at higher RH of 95 to 99 with with difference of around 0.01.

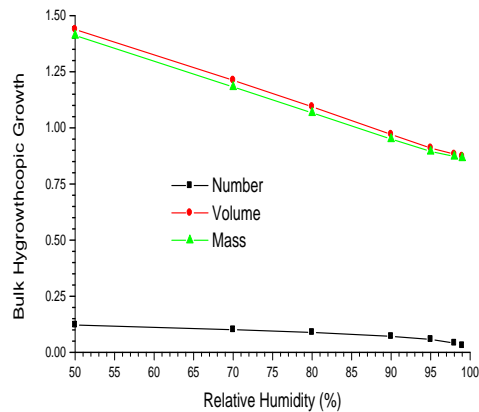


Figure 3. A graph of Bulk Hygroscopic Growth against Relative Humidity From the Data of Tables 2, 3 and 4.

From Figure 3, the plots can all satisfy power and linear relations with wavelengths, and the plot using volume is higher followed by mass with number being the least.

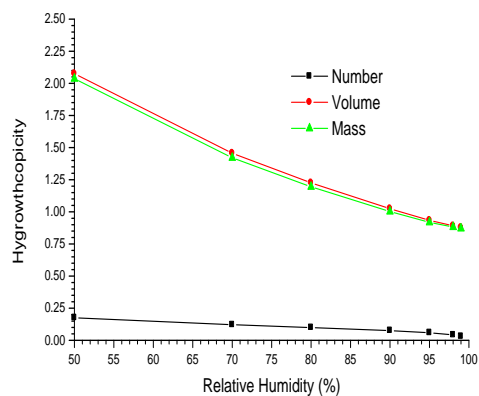


Figure 4. A graph of Hygroscopicity against Relative Humidity From the Data of Tables 2, 3 and 4.

From Figure 4, the plots can all satisfy power and linear relations with wavelengths, and the plot using volume is higher followed by mass with number being the least.

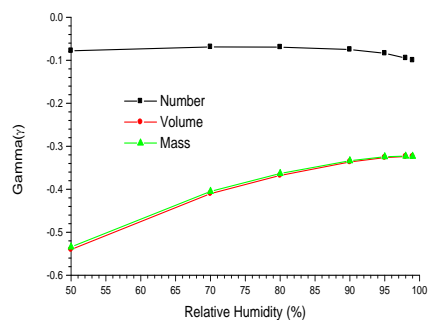


Figure 5. A graph of  $\gamma$  against Relative Humidity From the Data of Tables 2, 3 and 4.

From Figure 5, it can be observe that all the plots can satisfy power law, and the plots using volume and mass mix ratios have higher values in magnitude compared to using number mix ratios, though volume is the highest

most especially at lower RHs.

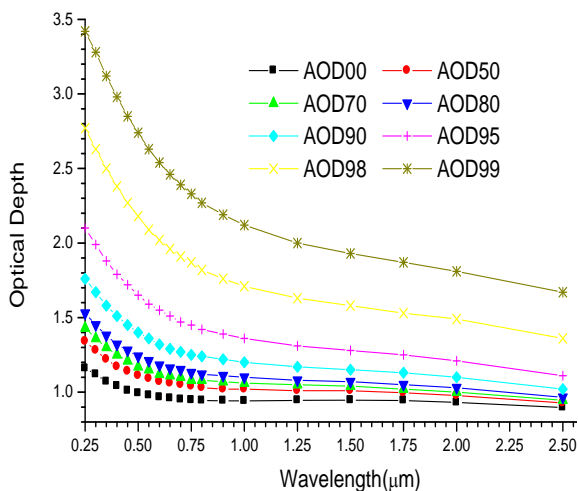


Figure 6: A graph of optical depth against wavelengths

From Figure 6, it can be observe that there is a slight increase in optical depth with the increase in RH at lower RH (0 to 80%) but at the delinquent point (90 to 99%) the increase is higher and in almost non-linear form. The behaviour of %RH with  $\lambda$ , shows higher values of optical depth at the near ultraviolet region, and this signifies the presence of fine particles due to the domonace of soot(see Table 1). But as the RH increases the presence of water solubles which are very hygroscopic and larger in size than soot continued to get dominance. Also as the RH increases, it shows that soot being smaller in size compared to water solubles and also being non-hygroscopic are acting as cloud condensation nuclei with respect to the water solubles.

The relation between optical depth and RHs using equation (17) are:

At  $\lambda=0.25 \mu$ ,  $A= 0.9704$ ,  $B= 0.8625$ ,  $R^2= 0.6059$

At  $\lambda=1.25 \mu$ ,  $A= 0.9274$ ,  $B= 0.4306$ ,  $R^2= 0.4888$

At  $\lambda=2.50 \mu$ ,  $A= 0.8721$ ,  $B= 0.3318$ ,  $R^2= 0.4098$

The relation between optical depth and RH shows decrease in  $R^2$  and the exponent B with the increase in wavelength, and this signifies the dominance of coarse particles.

Table 5: The results of the Angstrom coefficients for optical depth using equations (14), (15) and (16) at the respective relative humidities using regression analysis with SPSS16 for windows.

| RH (%) | Linear |          | Quadratic |            |            | Cubic  |            |            |            |
|--------|--------|----------|-----------|------------|------------|--------|------------|------------|------------|
|        | R2     | $\alpha$ | R2        | $\alpha_1$ | $\alpha_2$ | R2     | $\alpha_1$ | $\alpha_2$ | $\alpha_3$ |
| 0      | 0.7506 | 0.0885   | 0.9430    | -0.0580    | 0.0664     | 0.9805 | -0.0251    | 0.0290     | -0.0491    |
| 50     | 0.8738 | 0.1352   | 0.9692    | -0.1048    | 0.0663     | 0.9888 | -0.0712    | 0.0279     | -0.0503    |
| 70     | 0.9007 | 0.1574   | 0.9761    | -0.1264    | 0.0675     | 0.9904 | -0.0935    | 0.0299     | -0.0493    |
| 80     | 0.9193 | 0.1781   | 0.9810    | -0.1467    | 0.0684     | 0.9913 | -0.1154    | 0.0327     | -0.0468    |
| 90     | 0.9462 | 0.2185   | 0.9875    | -0.1874    | 0.0676     | 0.9926 | -0.1606    | 0.0370     | -0.0401    |
| 95     | 0.9667 | 0.2618   | 0.9921    | -0.2329    | 0.0629     | 0.9937 | -0.2154    | 0.0429     | -0.0262    |
| 98     | 0.9832 | 0.3072   | 0.9951    | -0.2842    | 0.0500     | 0.9951 | -0.2849    | 0.0508     | 0.0011     |
| 99     | 0.9888 | 0.3191   | 0.9955    | -0.3013    | 0.0388     | 0.9964 | -0.3174    | 0.0572     | 0.0241     |

From Table 5, it can be observe that the plot at 0% RH is very much less than 1, and this denotes the heavy dominance of coarse particles. But as the RH increases, since water soluble and sea salt accumulation are very hygroscopic despite being in small quantity they help in increasing the scattering with the increase in RH more at shorter wavelength and this is what caused the  $\alpha$  to also increase with the increase in RH. From the quadratic part the sign of  $\alpha_2$  (positive) signifies the dominance of coarse particles and its values increase with the increase in RH, until at the delinquent points (90 to 99%) when the curvature decreased with the increase in RH. The cubic part signifies mode distributions as bi-modal with the dominance of coarse particles.

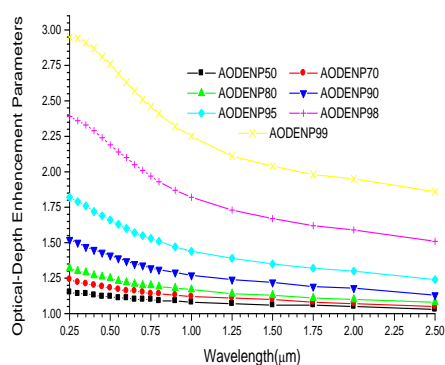


Figure 7: A graph of enhancement parameter for optical depth against wavelengths

From Figure 7, at lower RHs (50 to 80%), the enhancement is very small, this is in line with what can be observed most especially in Tables 3 and 4. But as from 90 to 99% RH it can be observe that there ia a non-linear increase of the enhancement factor (Tables 3 and 4). Its dependence on the wavelength shows that dominance of non-hygroscopic nature of the soot.

The results of the fitted curves of equations (10) and (12) are presented as follows;

For a single parameter using equation (10).

$$\text{At } \lambda=0.25 \mu, \gamma= 0.2159, R^2= 0.9909$$

$$\text{At } \lambda=0.45 \mu, \gamma= 0.1980, R^2= 0.9810$$

$$\text{At } \lambda=0.55 \mu, \gamma= 0.1872, R^2= 0.9761$$

$$\text{At } \lambda=0.70 \mu, \gamma= 0.1716, R^2= 0.9715$$

$$\text{At } \lambda=1.25 \mu, \gamma= 0.1347, R^2= 0.9593$$

$$\text{At } \lambda=2.50 \mu, \gamma= 0.1013, R^2= 0.9088$$

For two parameters using equation (12).

$$\text{At } \lambda=0.25 \mu, a= 0.9161, b= -0.2433, R^2= 0.9845$$

$$\text{At } \lambda=0.45 \mu, a= 0.8848, b= -0.2363, R^2= 0.9741$$

$$\text{At } \lambda=0.55 \mu, a= 0.8788, b= -0.2277, R^2= 0.9683$$

$$\text{At } \lambda=0.70 \mu, a= 0.8794, b= -0.2118, R^2= 0.9623$$

$$\text{At } \lambda=1.25 \mu, a= 0.8864, b= -0.1725, R^2= 0.9494$$

$$\text{At } \lambda=2.50 \mu, a= 0.8680, b= -0.1457, R^2= 0.9122$$

From both one and two parameters, it can be observe that the exponent decrease with the increase in wavelength. This is very much in agreement with what can be observe in Fig.7, that the relation between enhancement and RH is non-linear. The decrease in the exponent with the increase in wavelength reflects the increase in the dominance of non-hygroscopic particles.

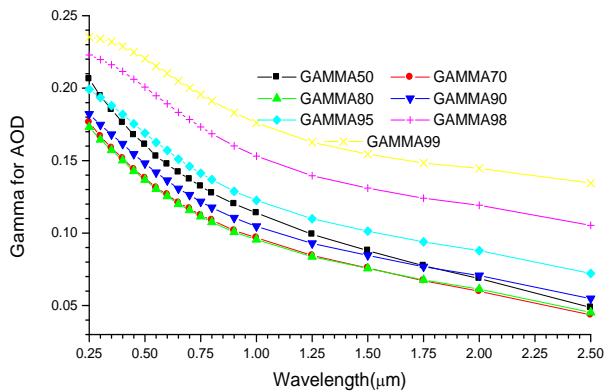


Figure 8 a graph of  $\gamma$  against wavelength using equation (11)

From Figure 8, it can be observe that the humidification factor decreases with the increase in wavelengths. The plot of  $\gamma$  at 50% RH is steeper. This shows the little concentration of fine particles. The decrease in the steepness occurred because of the increase in the hygroscopic growth due to the presence of water soluble and sea salt accumulation mode.

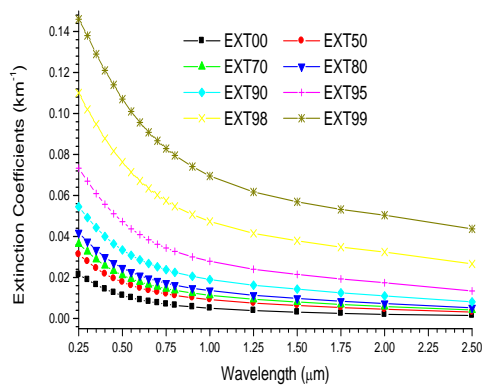


Figure 9: A graph of extinction coefficients against wavelengths

From Figure 9, it can be observe that the plots are similar to the plots in Figure 6, although there are some slight differences at the plots of 0, 50 and 70. They all satisfy power law. The relation between extinction and RHs using equation (17) are:

$$\text{At } \lambda=0.25 \mu, A= 0.0163, B= 1.6281, R^2= 0.7139$$

$$\text{At } \lambda=1.25 \mu, A= 0.0027, B= 2.3644, R^2= 0.7566$$

$$\text{At } \lambda=2.50 \mu, A= 0.0009, B= 2.8820, R^2= 0.7397$$

The decrease in A and increase in B with  $\lambda$ , shows the presence of fine particles that are responsible for more scattering at shorter wavelength, but shows the dominance of coarse particles because, soot despite being smaller but act as a cloud condensation nuclei. The relation between extinction coefficient and RH shows increase in the exponent and good values of  $R^2$ .

Table 6: The results of the Angstrom coefficients for extinction coefficient using equations (14), (15) and (16) at the respective relative humidities using regression analysis with SPSS16 for windows.

| RH (%) | Linear |        | Quadratic |            |            | Cubic  |            |            |            |
|--------|--------|--------|-----------|------------|------------|--------|------------|------------|------------|
|        | R2     | A      | R2        | $\alpha_1$ | $\alpha_2$ | R2     | $\alpha_1$ | $\alpha_2$ | $\alpha_3$ |
| 0      | 0.9951 | 1.1776 | 0.9995    | -1.2309    | -0.1161    | 0.9995 | -1.2379    | -0.1081    | 0.0105     |
| 50     | 0.9942 | 0.9674 | 0.9980    | -1.0078    | -0.0880    | 0.9986 | -0.9677    | -0.1338    | -0.0601    |
| 70     | 0.9945 | 0.9166 | 0.9975    | -0.9510    | -0.0750    | 0.9982 | -0.9098    | -0.1220    | -0.0616    |
| 80     | 0.9949 | 0.8765 | 0.9973    | -0.9059    | -0.0639    | 0.9980 | -0.8672    | -0.1080    | -0.0579    |
| 90     | 0.9959 | 0.8035 | 0.9973    | -0.8234    | -0.0433    | 0.9977 | -0.7964    | -0.0742    | -0.0404    |
| 95     | 0.9970 | 0.7271 | 0.9975    | -0.7387    | -0.0252    | 0.9976 | -0.7313    | -0.0337    | -0.0111    |
| 98     | 0.9974 | 0.6241 | 0.9974    | -0.6279    | -0.0081    | 0.9979 | -0.6507    | 0.0179     | 0.0341     |
| 99     | 0.9964 | 0.5452 | 0.9964    | -0.5449    | 0.0007     | 0.9985 | -0.5867    | 0.0484     | 0.0625     |

From Table 6, the values of  $\alpha$  at 0% RH signifies the dominance of fine particles due to the dominance of soot because it has the highest number concentration as shown in Table 1. But as the RH increases the values continue to decrease, because of the presence of water soluble and sea salt accumulation mode that are very hygroscopic and soot as cloud condensation nuclei, which cause the size of the particles to increase with the increase in RH as shown in Table 2, 3 and 4. From the quadratic part,  $\alpha_2$  continues to decrease in magnitude with the increase in RH, this also signifies increase in the dominance of more coarse particles with the increase in RH. The cubic part signifies mode distributions as bi-modal with the dominance of coarse particles.

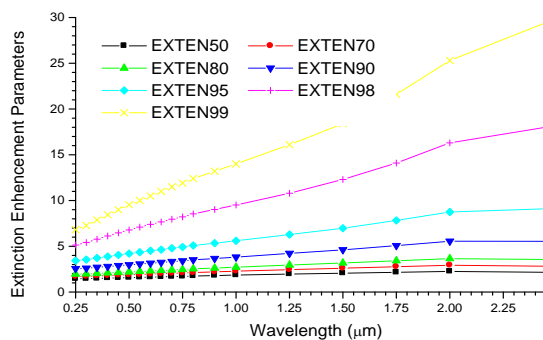


Figure 10: A graph of enhancement parameter for extinction coefficients against wavelengths

Figure 10, shows that the enhancement factors increase with the increase in RH and wavelengths. This shows the dominance of large and hygroscopic particles of water soluble and sea salt accumulation mode.

The results of the fitted curves of equations (10) and (12) using the data from the plots of figure 10 are presented as follows;

For a single parameter using equation (10).

At  $\lambda=0.25 \mu$ ,  $\gamma= 0.4174$ ,  $R^2= 0.9990$

At  $\lambda=0.45 \mu$ ,  $\gamma= 0.4762$ ,  $R^2= 0.9989$

At  $\lambda=0.55 \mu$ ,  $\gamma= 0.5008$ ,  $R^2= 0.9986$

At  $\lambda=0.70 \mu$ ,  $\gamma= 0.5716$ ,  $R^2= 0.9715$

At  $\lambda=1.25 \mu$ ,  $\gamma= 0.6188$ ,  $R^2= 0.9955$

At  $\lambda=2.50 \mu$ ,  $\gamma= 0.7481$ ,  $R^2= 0.9972$

For two parameters using equation (12).

At  $\lambda=0.25 \mu$ ,  $a= 1.0519$ ,  $b= -0.4015$ ,  $R^2= 0.9972$

At  $\lambda=0.45 \mu$ ,  $a= 1.0551$ ,  $b= -0.4594$ ,  $R^2= 0.9963$

At  $\lambda=0.55 \mu$ ,  $a= 1.0753$ ,  $b= -0.4781$ ,  $R^2= 0.9962$

At  $\lambda=0.70 \mu$ ,  $a= 1.1183$ ,  $b= -0.4973$ ,  $R^2= 0.9964$

At  $\lambda=1.25 \mu$ ,  $a= 1.2645$ ,  $b= -0.5453$ ,  $R^2= 0.9975$

At  $\lambda=2.50 \mu$ ,  $a= 1.2318$ ,  $b= -0.6828$ ,  $R^2= 0.9969$

From both the one and two parameters, it can be observe that the humidification factor and the exponent b all increase in magnitude with the increase in wavelengths. This signifies the good hygroscopic behavior and the dominance of water soluble and sea salt accumulation mode particles.

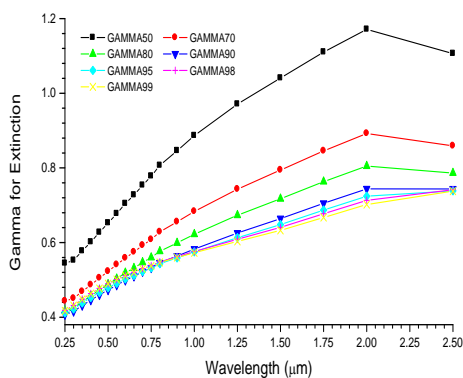


Figure 11: a graph of  $\gamma$  against wavelengths using equation (11).

Figure 11 shows that  $\gamma$  for the extinction decreases with the increase in RH most especially at RHs of 50, 70, 80 and 90, but the  $\gamma$  at the delinquent points 95 to 99% RH, it can be observe that the difference is not much.

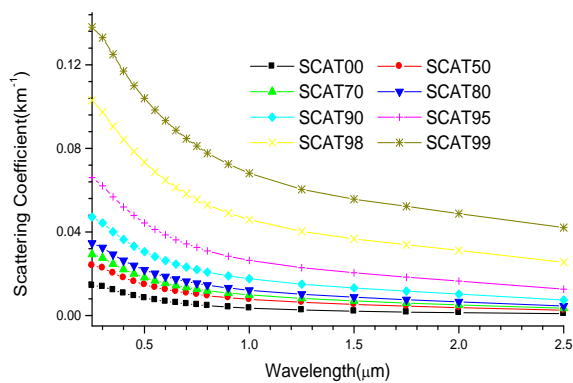


Figure 12: A graph of scattering coefficients against wavelengths

Figures 12 shows that the plots are similar to the plots of Fig.9.

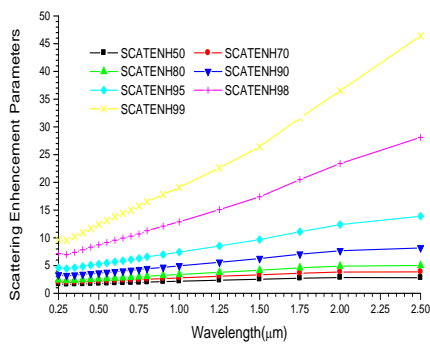


Figure 13: A graph of scattering enhancement against wavelengths

Figure 13 shows similar behavior with figure 10. This shows that the presence of water soluble and sea salt being very hygroscopic and soot acting as a cloud condensation nuclei, contributed to scattering and extinction enhancement being higher at higher wavelength.

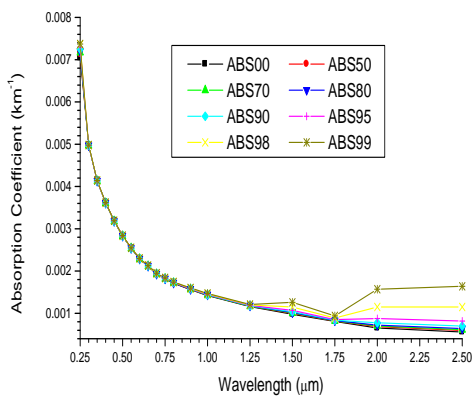


Figure 14: A graph of absorption coefficients against wavelengths

Figure 14, shows that absorption coefficients is independent of RH at the spectral wavelengths of 1.25 to 2.50  $\mu\text{m}$ , there is an increase of the coefficient with RH most especially at higher values of wavelength and RH.. The changes are more noticeable at the delinquent point (95 to 99%) RH. Its dependence with the wavelength shows that the plot can satisfy power law most especially at lower RH and wavelength. Also as from 0.25 to 2.50 it can be seen that the power law decreases with the increase in RH and wavelength.

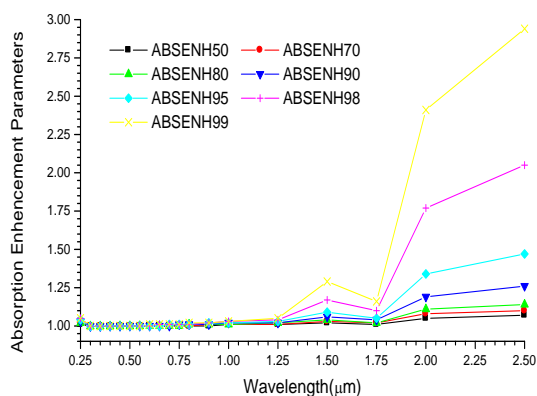


Figure 15: A graph of absorption enhancement against wavelengths

Figure 15 shows that the enhancement for absorption is negligible at shorter wavelengths, but became more

noticeable with the increase in wavelengths and relative humidity. This signifies the dominance of coarse mode particles.

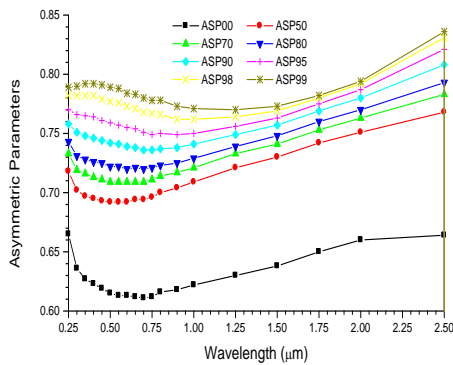


Figure 16: A graph of Asymmetric parameter against wavelengths

Figure 16 shows that the asymmetric parameter increases with the increase in RH and is much more at larger wavelengths.

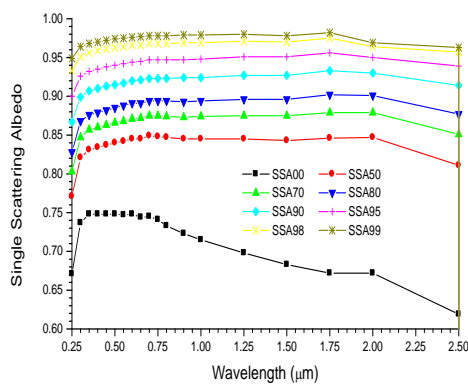


Figure 17: A graph of Single Scattering albedo against wavelengths

Figure 17 shows that single scattering albedo increases with the increase in RH, and this shows that scattering increases more than absorption with the increase in RH. At 0% RH, there is more absorption at shorter wavelength and this is due to the dominance of soot. But as the RH increases the soot act as the cloud condensation nuclei, where most hygroscopic particles stuck to them, and this is what caused the decrease in the absorption.

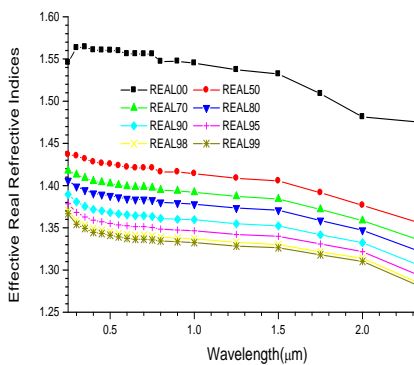


Figure 18: A plot of real effective refractive indices against wavelength using equation 18.

Figure 18 shows that the effective refractive indices decrease with the increase in RH. At 0% RH it can be seen that the effective refractive indices are higher. This is due to the dominance of soot particles that have higher number concentration and real refractive indices. As the RH increases, the water having lower refractive indices continue to decrease the refractive indices as the RH increased. Its behavior with wavelengths (i.e. not being constant) shows the dominance of non-spherical particles.

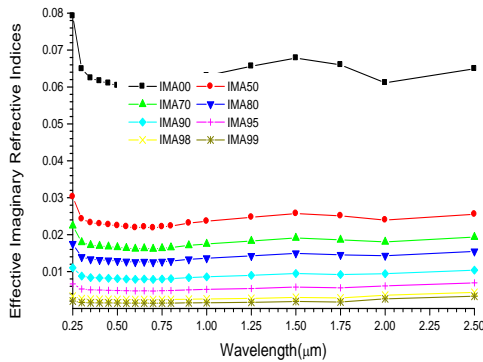


Figure 19: A plot of imaginary effective refractive indices against wavelength using equation 18.

Figure 19 shows decrease in the effective imaginary refractive indices with the increase in RH. The behavior of the plots being almost straight line with the increase in RH and wavelength shows the possibility of the mixture to be internally mixed and this can be attributed to the increase in the dominance of water solubles and sea-salt that are acting as a cloud condensation nuclei.

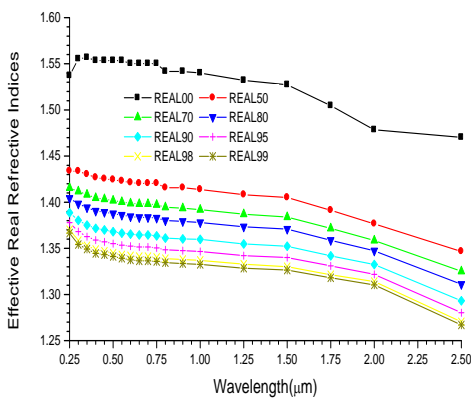


Figure 20: A plot of real effective refractive indices against wavelength using equation 20.

Figure 20 shows that the plots are similar to those of figure 18.

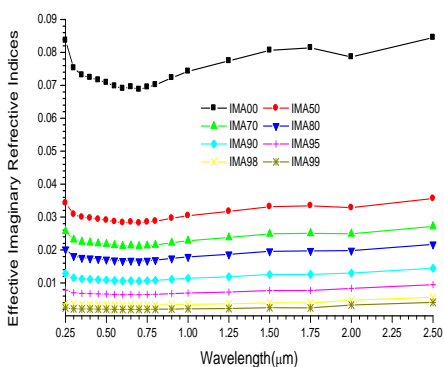


Figure 21: A plot of imaginary effective refractive indices against wavelength using equation 20.

Figure 21 shows by observation that the plots are similar to those of figure 19.

#### 4. Conclusion

From the behavior of the parameters observed from Tables 2, 3 and 4 and Figures 1, 2, 3, 4 and 5 they show that volume and mass mix ratios are more important in describing some microphysical properties of mixtures aerosols with respect to RHs.

From optical properties it can be concluded that increase in effective radii and hygroscopic growth of the mixture reveal an immense potential of light scattering enhancement.

From the  $gf_{mix}(RH)$  observed, it is assumed that the high number fraction of non-sea salt sulphate particles (NSS) is responsible for its high value.

It shows that volume and mass mix ratios can be more important in describing the hygroscopic and the Bulk Hygroscopicity factor (B)

It shows that increase in RH increases forward scattering because particle growth enhances forward diffraction (Liou, 2002) for smaller particles while in larger particles it causes increase in the backward scattering. It also shows that the mixture is internally mixed for smaller particles because of the increase in forward scattering as a result of the hygroscopic growth (Wang and Martin, 2007). The behavior of internal mixing can be attributed to the dominance of water soluble.

The relative importance of the humidity dependences of particle size and index of refraction on the aerosol scattering coefficient for a given substance depends on RH and on the sizes of the particles that provide the dominant contribution to the scattering.

These hygroscopic growth behaviors also reveal an immense potential of light scattering enhancement in the forward direction at high humidity and the potential for being highly effective cloud condensation nuclei.

It finally shows that marine aerosols are dominated by non-spherical particles.

Finally, the data fitted our models very and can be used to extrapolate the hygroscopic growth and enhancement parameters at any RH.

The importance of determining  $gf_{mix}(RH)$  as a function of RH and volume fractions, mass fractions and number fractions, and enhancement parameters as a function of RH and wavelengths can be potentially important because it can be used for efficiently representing aerosols-water interactions in global models.

The refractive index is highly variable depending on the chemical compositions of aerosols (d'Almeida et al., 1991).

#### References

- Angstrom, A. (1961): Techniques of Determining the Turbidity of the Atmosphere, *Tellus*, 13, 214–223.
- Aspens D. E. (1982), Local-field effect and effective medium theory: A microscopic perspective *Am. J. Phys.* 50, 704-709.
- Birmili, W., Nowak, A., Schwirn, K., Lehmann, K. et al. (2004) A new method to accurately relate dry and humidified number size distributions of atmospheric aerosols. *Journal of Aerosol Science* 1, 15–16, Abstracts of EAC, Budapest 2004.
- Cheng, Y. F., Wiedensohler, A., Eichler, H., Heintzenberg, J., Tesche, M., Ansmann, A., Wendisch, M., Su, H., Althausen, D., Herrmann, H., Gnauk, T., Brüggemann, E., Hu, M., and Zhang, Y. H.: Relative humidity dependence of aerosol optical properties and direct radiative forcing in the surface boundary layer at Xinken in Pearl River Delta of China: An observation based numerical study, *Atmos. Environ.*, 42, 6373–6397,

- 2008.
- Christensen, S. I. and Petters, M. D. (2012). The role of temperature in cloud droplet activation. *J. Phys. Chem. A* 116(39): 9706–9717.
- Clarke, A., et al. (2007). Biomass burning and pollution aerosol over North America: Organic components and their influence on spectral optical properties and humidification response, *J. Geophys. Res.*, 112, D12S18, doi:10.1029/2006JD007777.
- d’Almeida, G. A., P. Koepke, and E. P. Shettle (1991), *Atmospheric Aerosols: Global Climatology and Radiative Characteristics*, 561 pp., A. Deepak, Hampton, Va
- d’Almeida, G. A., P. Koepke, and E. P. Shettle, *Atmospheric Climatology and Radiative Characteristics*, 561 pp., A. Deepak, Hampton, Va., 1991.
- Doherty, et al., (2005). A comparison and summary of aerosol optical properties as observed in situ from aircraft, ship, and land during ACE-Asia. *Journal of Geophysical Research* 110, D04201.
- Duplissy J., P. F. DeCarlo, J. Dommen, M. R. Alfarra, A. Metzger, I. Barmadimos, A. S. H. Prevot, E. Weingartner, T. Tritscher, M. Gysel, A. C. Aiken, J. L. Jimenez, M. R. Canagaratna, D. R. Worsnop, D. R. Collins, J. Tomlinson, and U. Baltensperger, Relating hygroscopicity and composition of organic aerosol particulate matter *Atmos. Chem. Phys.*, 11, 1155–1165, 2011 [www.atmos-chem-phys.net/11/1155/2011/](http://www.atmos-chem-phys.net/11/1155/2011/) doi:10.5194/acp-11-1155-2011.
- Eck, T. F., Holben, B. N., Reid, J. S., Dubovic, O., Smirnov, A., O’Neil, N. T., Slutsker, I., and Kinne, S.: Wavelength dependence of the optical depth of biomass burning, urban, and desert dust aerosols, *J. Geophys. Res.*, 104(D24), 31 333–31 349, 1999.
- Gasso S., et al. (2000), Influence of humidity on the aerosol scattering coefficient and its effect on the upwelling radiance during ACE-2, *Tellus, Ser. B*, 52, 546 – 567.
- Gysel, M., McFiggans, G. B., and Coe, H.: Inversion of tandem differential mobility analyser (TDMA) measurements, *J. Aerosol Sci.*, 40, 134–151, 2009.
- Hanel, G. (1976). The Properties of Atmospheric Aerosol Particles as Functions of Relative Humidity at Thermodynamic Equilibrium with Surrounding Moist Air. In *Advances in Geophysics*, Vol. 19, H. E. Landsberg and J. Van Mieghem, eds., Academic Press, New York, pp. 73–188.
- Heller, W. (1945), The determination of refractive index of colloidal particles by means of a new mixture rule or from measurements of light scattering, *Phys. Rev.*, 68, 5 – 10.
- Hess M., Koepke P., and Schult I (May 1998), Optical Properties of Aerosols and Clouds: The Software Package OPAC, *Bulletin of the American Met. Soc.* 79, 5, p831-844.
- Jeong M. J, Li Z., Andrews E., Tsay S. C., (2007) Effect of aerosol humidification on the column aerosol optical thickness over the Atmospheric Radiation Measurement Southern Great Plains site, *J. Geophys. Res.*, 112, D10202, doi:10.1029/2006JD007176.
- Kammermann, L., Gysel, M., Weingartner, E., and Baltensperger, U.: 13-month climatology of the aerosol hygroscopicity at the free tropospheric site Jungfraujoch (3580 m a.s.l.), *Atmos. Chem. Phys.*, 10, 10717–10732, doi:10.5194/acp-10-10717-2010, 2010.
- Kaskaoutis, D. G. and Kambezidis, H. D. (2006): Investigation on the wavelength dependence of the aerosol optical depth in the Athens area, *Q. J. R. Meteorol. Soc.*, 132, 2217–2234,.
- Kasten, F.: Visibility forecast in the phase of pre-condensation, *Tellus*, XXI, 5, 631–635, 1969.
- Kaufman, Y. J. (1993), Aerosol optical thickness and atmospheric path radiance, *J. Geophys. Res.*, 98, 2677-2992.
- King, M. D. and Byrne, D. M. (1976): A method for inferring total ozone content from spectral variation of total optical depth obtained with a solar radiometer, *J. Atmos. Sci.*, 33, 2242–2251.
- Kohler, H.: The nucleus and growth of hygroscopic droplets, *Trans. Faraday Soc.*, 32, 1152–1161, 1936.
- Lorentz, H. A. (1880). Ueber die Beziehung zwischen der Fortpflanzungsgeschwindigkeit des Lichtes und der Körperdichte. *Ann. Phys. Chem.* 9, 641–665.
- Lorenz, L. (1880). Ueber die Refractionconstante. *Ann. Phys. Chem.* 11, 70–103.
- Martinez-Lozano, J.A., Utrillas, M.P., Tena, F., Pedros, R., Canada, J., Bosca, J.V., Lorente, J., (2001). Aerosol optical characteristics from summer campaign in an urban coastal Mediterranean area. *IEEE Transactions on Geoscience and Remote Sensing* 39, 1573–1585.
- Meier J., B. Wehner, A. Massling, W. Birmili, A. Nowak, T. Gnauk, E. Brüggemann, H. Herrmann, H. Min, and A. Wiedensohler Hygroscopic growth of urban aerosol particles in Beijing (China) during wintertime: a comparison of three experimental methods, *Atmos. Chem. Phys.*, 9, 6865–6880, 2009 [www.atmos-chem-phys.net/9/6865/2009/](http://www.atmos-chem-phys.net/9/6865/2009/)
- Meyer, N. K., Duplissy, J., Gysel, M., Metzger, A., Dommen, J., Weingartner, E., Alfarra, M. R., Prevot, A. S. H., Fletcher, C., Good, N., McFiggans, G., Jonsson, A. M., Hallquist, M., Baltensperger, U., and Ristovski, Z. D. (2009): Analysis of the hygroscopic and volatile properties of ammonium sulphate seeded and unseeded

- SOA particles, *Atmos. Chem. Phys.*, 9, 721–732, doi:10.5194/acp-9-721-2009.
- O'Neill, N. T., Dubovic, O., and Eck, T. F. (2001): Modified Angstrom exponent for the characterization of submicrometer aerosols, *Appl. Opt.*, 40(15), 2368–2375.
- O'Neill, N. T., Eck, T. F., Smirnov, A., Holben, B. N., and Thulasiraman, S.: Spectral discrimination of coarse and fine mode optical depth, *J. Geophys. Res.*, 198(D17), 4559, doi:10.1029/2002JD002975, 2003.
- Pedros, R., Martinez-Lozano, J. A., Utrillas, M. P., Gomez-Amo, J. L., and Tena, F. (2003): Column-integrated aerosol, optical properties from ground-based spectroradiometer measurements at Barrax (Spain) during the Digital Airborne Imaging Spectrometer Experiment (DAISEX) campaigns, *J. Geophys. Res.*, 108(D18), 4571, doi:10.1029/2002JD003331.
- Petters, M. D. and Kreidenweis, S. M. (2007). A single parameter representation of hygroscopic growth and cloud condensation nucleus activity. *Atmos. Chem. Phys.* 7(8): 1961–1971.
- Petters, M. D., Wex, H., Carrico, C. M., Hallbauer, E., Massling, A., McMeeking, G. R., Poulain, L., Wu, Z., Kreidenweis, S. M., and Stratmann, F.: Towards closing the gap between hygroscopic growth and activation for secondary organic aerosol: Part 2 theoretical approaches, *Atmos. Chem. Phys.*, 9, 3999–4009, doi:10.5194/acp-9-3999-2009, 2009.
- Putaud, J.-P.: Interactive comment on “Aerosol hygroscopicity at Ispra EMEP-GAW station” by M. Adam et al., *Atmos. Chem. Phys. Discuss.*, 12, C1316–C1322, 2012.
- Quinn, P. K., et al. (2005), Impact of particulate organic matter on the relative humidity dependence of light scattering: A simplified parameterization, *Geophys. Res. Lett.*, 32, L22809, doi:10.1029/2005GL024322.
- Randles, C. A., Russell L. M. and Ramaswamy V. (2004) Hygroscopic and optical properties of organic sea salt aerosol and consequences for climate forcing, *Geophysical Research Letters*, Vol. 31, L16108, doi:10.1029/2004GL020628.
- Rissler, J., Svenningsson, B., Fors, E. O., Bilde, M., and Swietlicki, E.: An evaluation and comparison of cloud condensation nucleus activity models: Predicting particle critical saturation from growth at subsaturation, *J. Geophys. Res.*, 115, D22208, doi:10.1029/2010jd014391, 2010.
- Schmid, B., Hegg, D.A., Wang, J., Bates, D., Redemann, J., Russell, P.B., Livingston, J.M., Jonsson, H.H., Welton, E.J., Seinfeld, J.H., Flagan, R.C., Covert, D.S., Dubovik, O., Jefferson, A., (2003). Column closure studies of lower tropospheric aerosol and water vapor during ACE-Asia using airborne Sun photometer and airborne in situ and ship-based lidar measurements. *Journal of Geophysical Research* 108 (D23), 8656.
- Shettle, E. P., and R. W. Fenn (1979), Models for the aerosols of the lower atmosphere and the effects of humidity variations on their optical properties, Rep. no. AFGL-TR-79-0214, ERP No. 676, Air Force Geophys. Lab., Optical Phys. Div., Hanscom Air Force Base, Mass.
- Sjogren, S., Gysel, M., Weingartner, E., Baltensperger, U., Cubison, M. J., Coe, H., Zardini, A. A., Marcolli, C., Krieger, U. K., and Peter, T. (2007): Hygroscopic growth and water uptake kinetics of two-phase aerosol particles consisting of ammonium sulfate, adipic and humic acid mixtures, *J. Aerosol Sci.*, 38, 157–171, doi:10.1016/j.jaerosci.2006.11.005.
- Stock M., Y. F. Cheng, W. Birmili, A. Massling, B. Wehner, T. Muller, S. Leinert, N. Kalivitis, N. Mihalopoulos, and A. Wiedensohler, (2011) Hygroscopic properties of atmospheric aerosol particles over the Eastern Mediterranean: implications for regional direct radiative forcing under clean and polluted conditions, *Atmos. Chem. Phys.*, 11, 4251–4271, [www.atmos-chem-phys.net/11/4251/2011/](http://www.atmos-chem-phys.net/11/4251/2011/) doi:10.5194/acp-11-4251-2011
- Stokes, R. H. and Robinson, R. A. (1966): Interactions in aqueous nonelectrolyte solutions. I. Solute-solvent equilibria, *J. Phys. Chem.*, 70, 2126–2130.
- Swietlicki, E., Hansson, H., Hameri, K., Svenningsson, B., Massling, A., McFiggans, G., McMurry, P., Petaja, T., Tunved, P., Gysel, M., et al.: Hygroscopic properties of submicrometer atmospheric aerosol particles measured with H-TDMA instruments in various environments -A review, *Tellus B*, 60, 432-469, 2008.
- Topping, D. O., McFiggans, G. B., and Coe, H.: A curved multi-component aerosol hygroscopicity model framework: Part 1-Inorganic compounds, *Atmos. Chem. Phys.*, 5, 1205-1222, doi:10.5194/acp-5-1205-2005, 2005a
- Topping, D. O., McFiggans, G. B., and Coe, H.: A curved multicomponent aerosol hygroscopicity model framework: Part 2-Including organic compounds, *Atmos. Chem. Phys.*, 5, 1223-1242, doi:10.5194/acp-5-1223-2005, 2005b.
- Wang J. and Martin S. T. (2007) Satellite characterization of urban aerosols: Importance of including hygroscopicity and mixing state in the retrieval algorithms, *Journal Of Geophysical Research*, Vol. 112, D17203, doi:10.1029/2006JD008078.

The IISTE is a pioneer in the Open-Access hosting service and academic event management. The aim of the firm is Accelerating Global Knowledge Sharing.

More information about the firm can be found on the homepage:  
<http://www.iiste.org>

## CALL FOR JOURNAL PAPERS

There are more than 30 peer-reviewed academic journals hosted under the hosting platform.

**Prospective authors of journals can find the submission instruction on the following page:** <http://www.iiste.org/journals/> All the journals articles are available online to the readers all over the world without financial, legal, or technical barriers other than those inseparable from gaining access to the internet itself. Paper version of the journals is also available upon request of readers and authors.

## MORE RESOURCES

Book publication information: <http://www.iiste.org/book/>

## IISTE Knowledge Sharing Partners

EBSCO, Index Copernicus, Ulrich's Periodicals Directory, JournalTOCS, PKP Open Archives Harvester, Bielefeld Academic Search Engine, Elektronische Zeitschriftenbibliothek EZB, Open J-Gate, OCLC WorldCat, Universe Digital Library, NewJour, Google Scholar

